

Article

# Long-Term Regional Environmental Risk Assessment and Future Scenario Projection at Ningbo, China Coupling the Impact of Sea Level Rise

Yongjiu Feng<sup>1,2,\*</sup>, Qianqian Yang<sup>1</sup>, Xiaohua Tong<sup>1,\*</sup>, Jiafeng Wang<sup>3</sup>, Shurui Chen<sup>3</sup>,  
Zhenkun Lei<sup>3</sup> and Chen Gao<sup>3</sup>

<sup>1</sup> College of Surveying and Geo-Informatics, Tongji University, Shanghai 200092, China; 1810650@tongji.edu.cn

<sup>2</sup> School of Earth and Environmental Sciences, The University of Queensland, Brisbane, QLD 4072, Australia

<sup>3</sup> College of Marine Sciences, Shanghai Ocean University, Shanghai 201306, China; wangjf93024@163.com (J.W.); ChenSR96@outlook.com (S.C.); Leizhenk@outlook.com (Z.L.); gcjnws@163.com (C.G.)

\* Correspondence: y.feng1@uq.edu.au (Y.F.); xhtong@tongji.edu.cn (X.T.)

Received: 18 February 2019; Accepted: 8 March 2019; Published: 14 March 2019



**Abstract:** Regional environmental risk (RER) denotes potential threats to the natural environment, human health and socioeconomic development caused by specific risks. It is valuable to assess long-term RER in coastal areas with the increasing effects of global change. We proposed a new approach to assess coastal RER considering spatial factors using principal component analysis (PCA) and used a future land use simulation (FLUS) model to project future RER scenarios considering the impact of sea level rise (SLR). In our study, the RER status was classified in five levels as highest, high, medium, low and lowest. We evaluated the 30 m × 30 m gridded spatial pattern of the long-term RER at Ningbo of China by assessing its 1975–2015 history and projecting this to 2020–2050. Our results show that RER at Ningbo has increased substantially over the past 40 years and will slowly increase over the next 35 years. Ningbo’s city center and district centers are exposed to medium-to-highest RER, while the suburban areas are exposed to lowest-to-medium lower RER. Storm surges will lead to strong RER increases along the Ningbo coast, with the low-lying northern coast being more affected than the mountainous southern coast. RER at Ningbo is affected principally by the combined effects of increased human activity, rapid population growth, rapid industrialization, and unprecedented urbanization. This study provides early warnings to support practical regulation for disaster mitigation and environmental protection.

**Keywords:** regional environmental risk (RER) assessment; scenario projection; principal component analysis (PCA); storm surge; Ningbo

## 1. Introduction

Regional environmental risk (RER) denotes potential threats to the natural environment, human health and socioeconomic development caused by specific risks [1,2]. RER can be expressed by uncertainty in the consequence and degree of environmental damage [2]. For example, industrial and domestic wastes create potential environmental risks that may threaten the sustainability of urban systems [3,4]. Land-use change, accompanied by accelerating industrialization and urbanization, has led to the alteration of the natural environment and ecosystem degradation [5,6]. Intensified human impacts have led to accumulated greenhouse effects and global change, ultimately resulting in global warming and sea level rise (SLR) [7]. SLR increases the intensity and frequency of storm surges, intensifying RER in coastal areas that are significantly affected by inundation [8]. Coastal regions will

be exposed to increased RER because the ecosystems and environments are inherently vulnerable. It is therefore essential to consider the impact of SLR in long-term RER assessment and future scenario projection in coastal areas.

RER assessment is to synthetically evaluate the risk sources, risk receptors and risk retardation from a macro perspective [9,10], offering possible countermeasures that can reduce risks. Efforts have been made to the spatial and quantitative assessment of RER as it relates to specific combinations of risks. Aiming to develop risk-mitigation measures, modelers have assessed RER in inland and coastal zones regarding hazardous substances [11] and pollutants [9,12]. From a spatial perspective, a few publications have evaluated RER caused by multiple risk sources [13], metal in soil [14], vulnerable environmental factors [15] and toxic compounds [16]. These studies have mapped RER patterns to identify high-risk areas and support the formulation of sustainable development plans. In RER studies, a Pressure-State-Response (PSR) framework has commonly been applied to estimate the risk level [10,17], with the support of the analytical hierarchy process (AHP) and geographical information systems (GIS). The entropy method [18], fuzzy method [19] and expert evaluation method (EEM) [20] have also been applied to the assessment of ecological security related to RER. While AHP and EEM have been applied to evaluate RER patterns with the absence of prior knowledge of risk levels [17,21], they strongly depend on subjective model parameterization that can influence the credibility of the results. In coastal areas, the impacts of sea level rise on environments have commonly been studied using three basic approaches, i.e., behavior-oriented models [22], process-based models [23] and hybrid models [24]. McLeod et al. [25] summarized these coastal impact models and noted a few of them including inundation models (e.g., GIS), SLAMM, BTELSS, DIVA, and SimCLIM. These models can predict a wide range of coastal environments such as morphological evolution and estuarine sedimentation.

Despite considerable progress in the study of RER, improved assessment methods must consider other physical and socioeconomic driving forces, particularly because coastal environments are now substantially affected by global change and SLR. As a result, critical issues related to RER include: (1) objective parameterization for assessing spatial patterns of RER, (2) proper projection of future RER scenarios, and (3) comprehensive assessment of future RER patterns considering the influences of SLR and storm surges. In this study, storm surge refers to coastal flooding commonly associated with typhoons, heavy rainfall and extreme high tides [26], which may increase social vulnerability and environmental risks. To date, answers to these questions have not been adequately addressed, and further studies are needed for model development and integrated environmental management.

The objective of this study is to adequately address the above issues by developing new methods for assessing RER patterns and projecting their future scenarios. Our new assessment method is based on the principal component analysis (PCA). It is a dimensionality reduction method whose outputs are directly derived from the independent factors [27], leading to the objective definition of the effects of these factors. Land coverage indices and distance-based factors were applied as input variables for the modeling. These variables are representative of the land coverage status, human impacts, and socioeconomic aspect. Our new method also incorporates GIS to facilitate the spatial visualization [16,17,28–30] and the quantification [31–33] of RER status, providing a clearer understanding. We used a bottom-up cellular automata (CA) model to project future scenarios by processing the RER maps into categorical figures. CA models have been widely applied to simulate and predict spatiotemporal, dynamic phenomena [34,35]. The models can automatically update their transition rules during the simulation procedure, and have substantial advantages of categorical modeling in tessellated space but weak capabilities to model continuous value-based spatial phenomena [36]. We applied the future land use simulation (FLUS) model, a state-of-art CA tool for modeling complex land use change and spatiotemporal phenomena [35,37], to predict the RER future scenarios.

## 2. Methodology

### 2.1. Procedure

For modeling RER (Figure 1), we first used remote sensing imagery and vector maps to derive the factors impacting RER at Ningbo. Based on these factors, we then applied PCA to evaluate the present RER pattern in 2015 and to assess the past RER patterns for 1975, 1990 and 2006. Consequently, the FLUS model of spatial phenomena [35,37] was used to project before-inundation RER scenarios from 2020 to 2050. We then applied a GIS approach (inundation model) to evaluate after-inundation RER scenarios from 2020 to 2050, taking into account terrain (from a digital elevation model: DEM), SLR and storm surge. Our long-term RER assessment should help formulate more appropriate plans for regional development and environmental protection, and could help establish defensive measures to rehabilitate coastal environments by taking SLR into account.

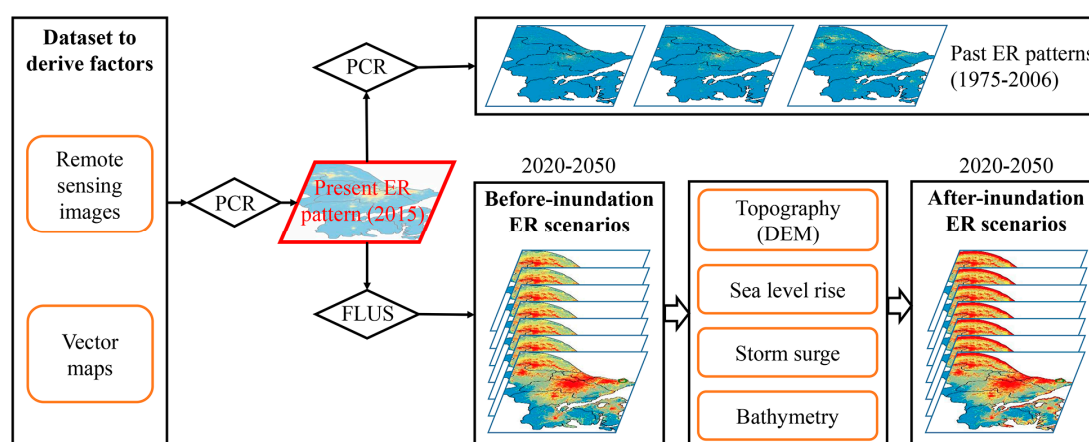


Figure 1. Workflow used in this study.

### 2.2. Study Area and Input Data

Ningbo is a port city situated in the middle of China's east coast (Figure 2a). The city covers 9816 km<sup>2</sup> and consists of two county-level cities (Cixi and Yuyao), two counties (Ninghai and Xiangshan), and six districts (Jinzhou, Haishu, Jiangbei, Zhenhai, Beilun and Fenghua) (Figure 2b). Haishu and Jinzhou constitute the Ningbo City center. Ningbo is an economic center of the southern wing of the Yangtze River Delta [38], and is the eastern departure port for the 'Marine Silk Road' on the Yongjiang River estuary.

As of 2015, Ningbo's population was ~7.8 million [39], and the annual GDP was ~801 billion Chinese Yuan (~121 billion USD) [39]. A vast population and a vibrant economy have resulted in high demand for commercial and residential space, leading to unprecedented land-use changes that pose serious challenges to ecosystems and the natural environment. Due to the major changes in land-use and environmental pressure, Ningbo has attracted attention from environmentalists and local authorities [40,41] and is of great interest to environmentalists, geographers and scientists [42,43].

We used graphic GIS datasets and remote sensing imagery (Table 1) to derive spatial factors influencing RER at Ningbo. The Ningbo City center and district/county centers were defined using administrative maps, which differ between 1975–1990 and 2006–2015. Four Landsat images were used to compute the normalized difference vegetation index (NDVI) and the normalized difference building index (NDBI). The terrain at Ningbo was stable over the past four decades, thus we used only the 2010 DEM to guide the impact of terrain on future RER scenarios.

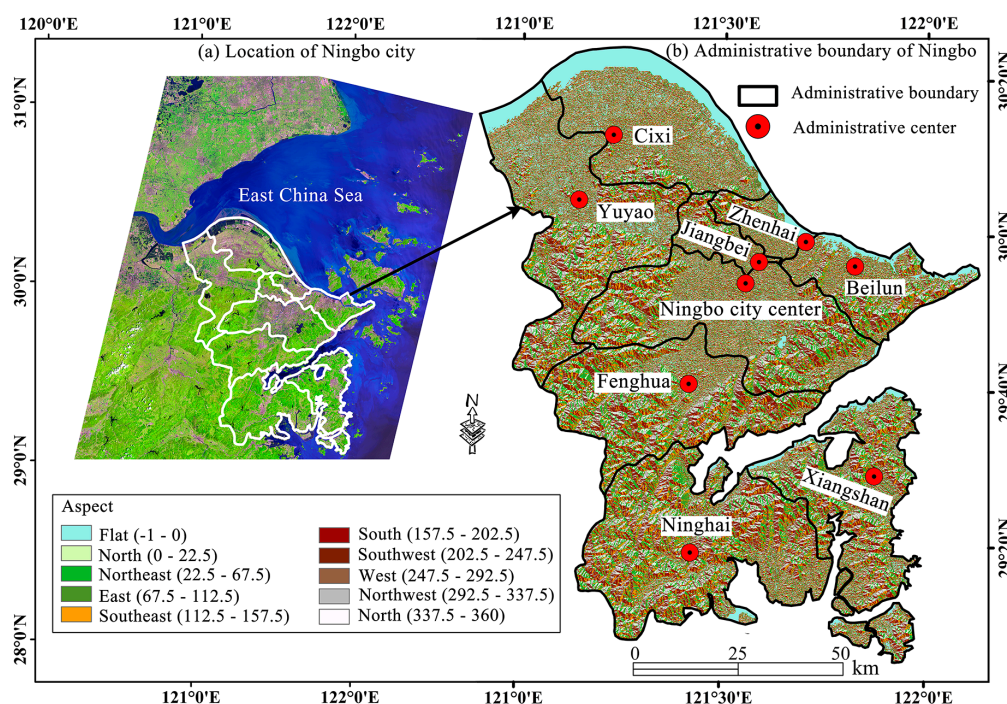


**Figure 2.** Location and administrative boundaries of Ningbo City: (a) false-color Landsat composite image for 2006; and (b) a 2010 map for terrain aspect reflected in 10 azimuthal categories.

**Table 1.** Spatial data and satellite imagery used in this study.

Raw Data	Type	Date	Description	Provider
Administrative maps	Graphic	1990, 2006	Administrative boundaries and centers	National Catalogue Service for Geographic Information ( <a href="http://www.webmap.cn">www.webmap.cn</a> )
Landsat-1 (MSS)	Image	1975.2	A remote sensing image for assessing vegetation coverage and built-up area	Open Spatial Data Sharing Project ( <a href="http://ids.ceode.ac.cn">ids.ceode.ac.cn</a> )
Landsat-5 (TM)	Image	1990.6	A remote sensing image for assessing vegetation coverage and built-up area	Open Spatial Data Sharing Project ( <a href="http://ids.ceode.ac.cn">ids.ceode.ac.cn</a> )
Landsat-5 (TM)	Image	2006.3	A remote sensing image for assessing vegetation coverage and built-up area	Open Spatial Data Sharing Project ( <a href="http://ids.ceode.ac.cn">ids.ceode.ac.cn</a> )
Landsat-8 (OLI)	Image	2015.1	A remote sensing image for assessing vegetation coverage and built-up area	Open Spatial Data Sharing Project ( <a href="http://ids.ceode.ac.cn">ids.ceode.ac.cn</a> )
ASTER GDEM	Image	2010.7	A map of Ningbo terrain	Geospatial Data Cloud ( <a href="http://gscloud.cn">gscloud.cn</a> )

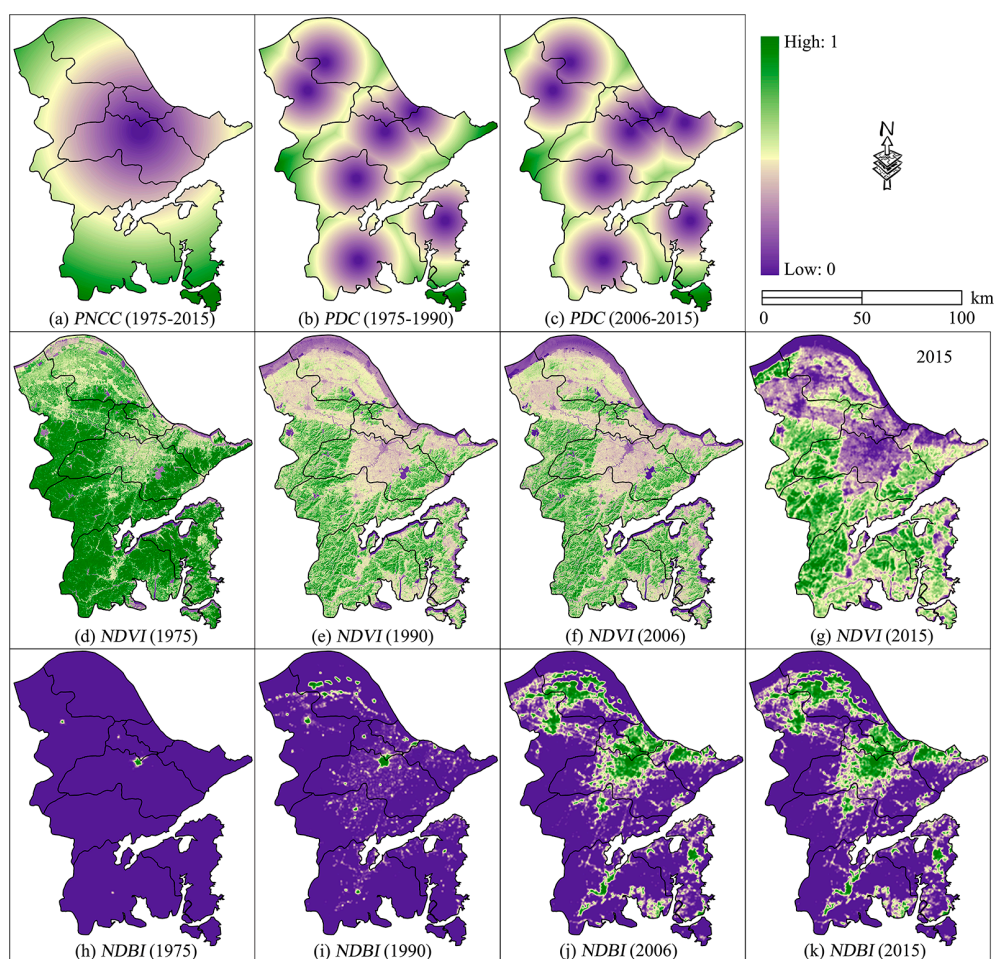
### 2.3. Input Variables

Increasing human demand for natural and land resources has put great pressure on the natural environment [44] from facility construction, landscape alteration, urban development and land reclamation [45,46]. This has led to global land-use change, reduction in vegetation coverage, and growth in built-up areas [47]. We selected four typical spatial influencing factors to evaluate RER patterns at Ningbo: proximity to Ningbo city center (PNCC), proximity to district centers (PDC), NDVI and NDBI, as defined in Table 2. Using the ArcGIS Euclidean Distance tool, we calculated PNCC and PDC to represent the distance from each pixel and its nearest city/district centers; using the ArcGIS Map Algebra tool, we computed NDVI and NDBI to describe the land coverage status.

**Table 2.** Selected spatial influencing factors for assessing regional environmental risk (RER) patterns in Ningbo.

Variable	Meaning	Purpose
PNCC	Proximity to Ningbo City center	Produce the distance to the Ningbo City center and evaluate its impact on the environments.
PDC	Proximity to district centers	Produce the distances to the district centers and evaluate their impact on the environments.
NDBI	Normalized difference built-up index	Produce the built-up density and evaluate its impact on the environments.
NDVI	Normalized difference vegetation index	Produce the vegetation coverage and evaluate its impact on the environments.

Ningbo City center and the district centers have the highest density of impervious surfaces, suggesting the major human alteration of the natural environments. The use of proximity factors is therefore effective in delineating RER caused by human disturbance. Generally, a higher PNCC (or PDC) suggests a lower building density and higher vegetation coverage, hence a weaker human impact and less-altered natural environments [20,21]. We produced one PNCC map and two PDC maps using the administrative maps in 1990 and 2006 (Figure 3a–c). These two factors are temporally stationary when including them to assess the past RER scenarios as well as projecting the before-inundation scenarios. The topo-bathymetry was considered for the after-inundation scenarios.

**Figure 3.** Maps of proximity factors, normalized difference vegetation index (NDVI) and normalized difference built-up index (NDBI) from 1975 to 2015 [21].

NDVI reflects vegetation coverage and is an important indicator of the integrity of ecological environments, with a higher NDVI indicating a less-altered natural environment [48]. Figure 3d–g shows a decline in vegetation coverage at Ningbo from 1975 to 2015. The built-up density reflects the intensity of human-disturbance and probably population density [49], and a higher built-up density suggests a greater human alteration of the natural environments [50]. Figure 3h–k shows the NDBI maps that measure the built-up density as an important indicator of human impacts, reflecting the status of human-made surfaces. The maps in Figure 3 were produced following Feng et al. [21].

Ningbo City center and the district centers have the highest density of impervious surfaces, suggesting the major human alteration of the natural environments. The use of proximity factors is therefore effective in delineating RER caused by human disturbance. Generally, a higher PNCC (or PDC) suggests a lower building density and higher vegetation coverage, hence a weaker human impact and less-altered natural environments [20,21]. We produced one PNCC map and two PDC maps using the administrative maps in 1990 and 2006 (Figure 3a–c). These two factors are temporally stationary when including them to assess the past RER scenarios as well as projecting the before-inundation scenarios. The topo-bathymetry was considered for the after-inundation scenarios.

NDVI reflects vegetation coverage and is an important indicator of the integrity of ecological environments, with a higher NDVI indicating less-altered natural environment [48]. Figure 3d–g shows a decline in vegetation coverage at Ningbo from 1975 to 2015. The built-up density reflects the intensity of human-disturbance and probably population density [49], and a higher built-up density suggests a greater human alteration of the natural environments [50]. Figure 3h–k shows the NDBI maps that measure the built-up density as an important indicator of human impacts, reflecting the status of human-made surfaces. The maps in Figure 3 were produced following Feng et al. [21].

#### 2.4. RER Assessment and Projection Methods

We summarized the RER assessment and projection methods in Table 3, then described them in detail in the following sub-sections.

**Table 3.** A summary of the indicators of the RER assessment and projection methods.

Item	Method	Indicator
Definition of five-level RER	Score classification	Lowest risk [0.0, 0.2), low risk [0.2, 0.4), medium risk [0.4, 0.6), high risk [0.6, 0.8), and highest risk [0.8, 1.0]
RER assessment method	Principal component analysis (PCA)	Total cumulative variance
RER projection method	Cellular automata (FLUS)	Kappa, overall accuracy, producer's accuracy, user's accuracy, omission error, and commission error

##### 2.4.1. Definition of Five-Level RER Score

The RER score was defined as a real number in the range of [0, 1], where a smaller score denotes better environmental status. A risk score of 0 means that the natural environment is at zero risk with very high vegetation coverage and no pollution sources; a risk score of 1 indicates that the natural environment is at high risk and seriously damaged by high-density buildings. Artificial impervious surface area causes great environmental risks by altering the natural environment, reducing infiltration capacity, changing urban runoff, and aggravating urban water pollution. We categorized risk in five equally-spaced levels (Table 3) following earlier publications [20,21].

##### 2.4.2. Principal Component Analysis (PCA)

PCA identifies uncorrelated principal components from candidate factors using an orthogonal transformation that captures internal structural relationships among the factors [51]. The method processes the dataset without considering the dependent variables, and then estimates a weighting

factor for each. In this study, the RER score (the dependent variable) is unknown. As such, PCA is an objective parameterization method [52] that is particularly suitable for retrieving the weight of each RER factor, avoiding adverse negative effects that may be caused by subjective parameterization in methods like expert evaluation. Each principal component reflects one aspect of the independent variables, and all selected principal components should ideally explain more than 80% of these variables, with no information repeated [52].

In this study, the first three principal components of selected factors yielded the total cumulative variances of 82.2%, 82.7%, 90.0% and 87.7% for 1975, 1990, 2006 and 2015, successively. The weight of each factor was then defined by the first three principal components and represented as:

$$\begin{cases} F_{1975} = 1 - (0.531PNCC + 0.427PDC + 0.001NDBI + 0.689NDVI) \\ F_{1990} = 1 - (0.525PNCC + 0.409PDC + 0.015NDBI + 0.506NDVI) \\ F_{2006} = 1 - (0.511PNCC + 0.391PDC + 0.116NDBI + 0.484NDVI) \\ F_{2015} = 1 - (0.517PNCC + 0.377PDC + 0.095NDBI + 0.845NDVI) \end{cases} \quad (1)$$

where  $F_{year}$  represents the comprehensive RER score each year, and the items in brackets represent the integrity and goodness of the natural environments. A smaller parameter indicates a higher impact in affecting RER at Ningbo. The coefficients in Equation (1) show that NDBI is the dominant RER factor followed by PDC, PNCC and NDVI.

#### 2.4.3. Projection Method of RER Scenarios

We applied a FLUS model to project future RER scenarios at Ningbo from 2020 to 2050 at 5-year intervals. FLUS is an explicit modeling tool for simulating land-use change dynamics and spatial phenomena [35,37]. This model integrates interactions between top-to-bottom system dynamics (SD) and a bottom-to-top CA model to simulate spatial dynamics. It first uses SD to project the future dimensions of different types considering the effects of various driving factors, then allocates spatial change according to the quantity of each type using CA modeling. Here, FLUS was calibrated using candidate factors to simulate the 2015 RER and project future RER scenarios. We applied six accuracy and error indices (Table 3) to assess the 2015 simulation and validate the FLUS model [53].

#### 2.5. SLR Inundation Analysis

The IPCC fourth assessment report (AR4) shows that the average rate of global SLR was about 1.8 (1.3 to 2.3 range) mm per year from 1961 to 2003, and about 3.1 (2.4 to 3.8 range) mm per year from 1993 to 2003. The IPCC fifth assessment report (AR5) suggests that the global mean SLR rate was about 3 mm per year from 1993 to 2012. Both AR4 and AR5 demonstrate that global warming caused by human impacts is the main driver of SLR. The State Ocean Administration of China (SOAC) reported that the average sea level in China rose by 0.11 m from 1980 to 2005, and the rate was 3.7 mm per year from 1993 to 2010 [54]. This is faster than the global average SLR rate reported by IPCC. We applied the SOAC SLR estimate to assume that the maximum inundation of 10 m in Ningbo, thus evaluating the inundation-induced RER.

SLR exacerbates the frequency and intensity of storm surges [55,56], which are likely causes of damage and disaster in coastal areas. Storm surges accompanied by rising tides and heavy rainfalls lead to coastal flooding, with longer inundation hours implying deeper bathymetric inundation, thus greater environmental damage [26]. We assume that inundation time increases by 2 h if the surge-induced water level rises by 1-m bathymetry; conversely, it takes 2 h for the water level to drop by 1-m bathymetry. For flooded areas, more inundation hours imply higher RER. We also assume that the maximum water-level rise in Ningbo is 10 m, which is related to the inundation of 20 h. We categorized inundation risk into five levels according to the water-level rise and inundation hours with each 4-h (2-m bathymetry) inundation related to one inundation level. These risk levels are lowest, low, medium, high and highest, in ascending order. For instance, an inundation-time shorter

than 4 h is the lowest risk. Meanwhile, inundation produces pressure on the coastal environments and intensifies RER. We produced the inundation maps and assessed the inundation-induced RER considering the elevation, producing comprehensive RER maps that take into account the combined effects of human activities and SLR.

### 3. Results

#### 3.1. RER Spatial Patterns and Disparity

The four panels in Figure 4 show good environmental status in most areas in Ningbo, indicating only weak environmental risk in these areas; however, the RER deterioration is evident in Ningbo City center and the eight district centers.

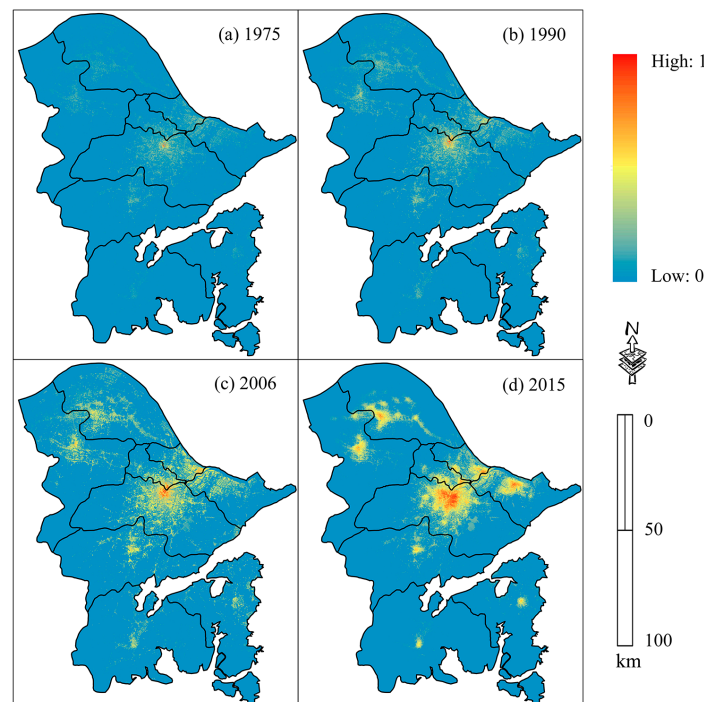


**Figure 4.** RER patterns at Ningbo for 1975 (a), 1990 (b), 2006 (c) and 2015 (d).

In 1975 and 1990, most areas had excellent environmental conditions, and only a small fraction (mainly in the Ningbo City center) had a higher ( $\sim 0.8$ ) RER. Figure 4a,b shows that the areas (in the district centers) with “medium” RER slightly expanded from 1975 to 1990. By 2006, there was further environmental deterioration, and areas with “lowest” RER expanded in the Ningbo City center (Figure 4c). Areas experiencing environmental degradation have spread in the district centers, including Cixi, Yuyao, Fenghua, and Zhenhai, all of which show evident increases in RER. By 2015, the environmental conditions in the Ningbo City center and the district centers of Cixi, Yuyao, Zhenhai and Beilun had deteriorated substantially, with the negative extent significantly expanded (Figure 4d). Among these sub-areas, Ningbo City center has experienced the highest RER increase, while Ninghai and Xiangshan experienced only marginal increases.

Figure 5 presents histograms of the RER scores in each of the four years with a bin width of 0.05. All four years show left-skewed and platykurtic distributions, where the highest frequency in 1975, 1990, 2006 and 2015 occurs between 0.05–0.10, 0.10–0.15, 0.3–0.35, and 0.3–0.35, respectively. During 1975–2015, the highest RER score increased from 0.28 to 0.91, and the mean RER score substantially increased from 0.08 to 0.40. These indicate a movement of the highest frequency towards a higher risk score, suggesting an increasing RER in Ningbo. The standard deviation has slightly increased from 0.03 to 0.13, implying an increasing spatial heterogeneity in RER over the past 40 years.

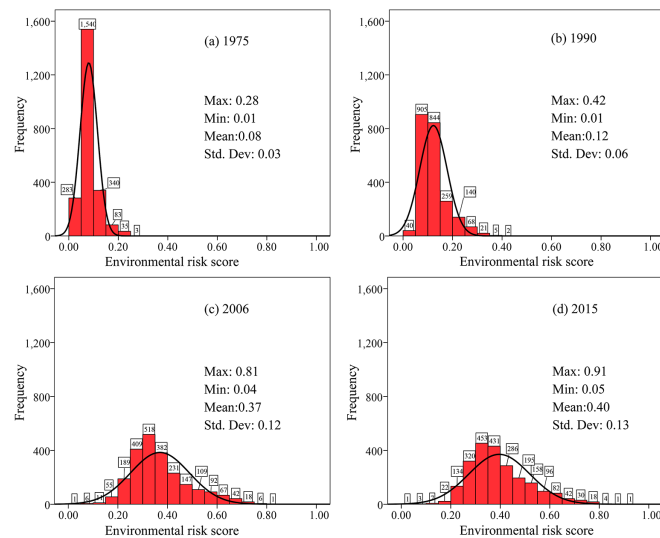


**Figure 5.** Frequency distribution of 1975 (a), 1990 (b), 2006 (c) and 2015 (d) RER scores, and the black curve is the best-fitted distribution.

### 3.2. Changes in RER Patterns

During all three periods, RER increased substantially (by up to 0.4) in the Ningbo City center and district centers where artificial building surfaces have been greatly developed (Figure 6). RER in other areas was unchanged, or in some cases was reduced by up to  $-0.4$ . There was a distinct risk-level change from 1975 to 1990, with higher risk levels found in the Ningbo City center and most district centers. The risk increases were spatially clustered and extended from 1990 to 2015, showing a similar tendency in risk change during all three time intervals. By comparison, those areas with increased risk during 2006–2015 were significantly larger than those during 1975–1990 and 1990–2006.

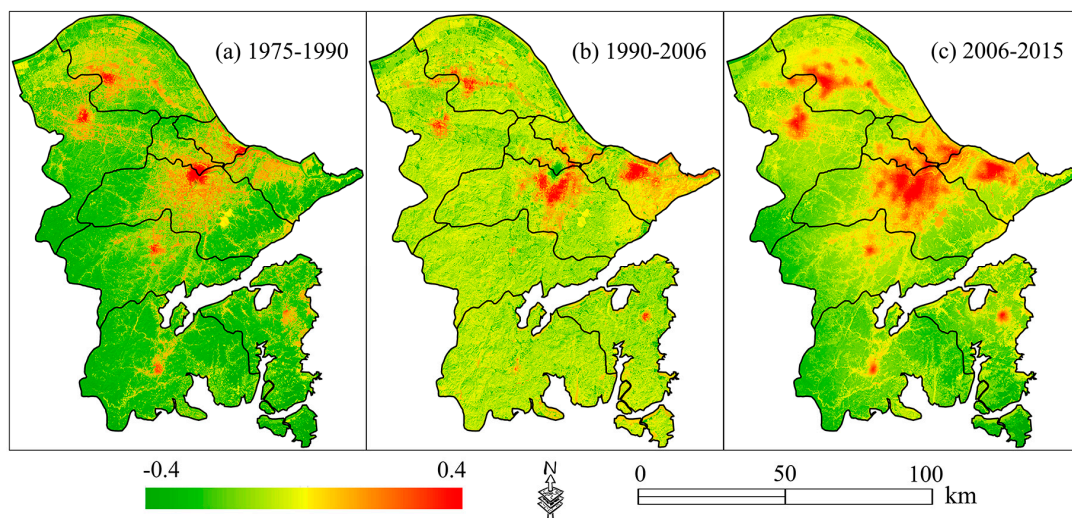


**Figure 6.** RER change at Ningbo: red denotes increased risk, yellow denotes persistent (steady) risk, green denotes decreased risk.

### 3.3. Future RER Scenarios

To forecast future RER scenarios for Ningbo, we calibrated the FLUS model using the five-level RER pattern in 2015 as the starting map and utilized four driving factors PDC, NDVI, NDBI, and PNCC as independent variables. A simulated 2015 RER map was then generated to validate the FLUS

model. Visual inspection (Figure 7) shows the similarity between the assessed RER pattern and the simulated RER pattern.

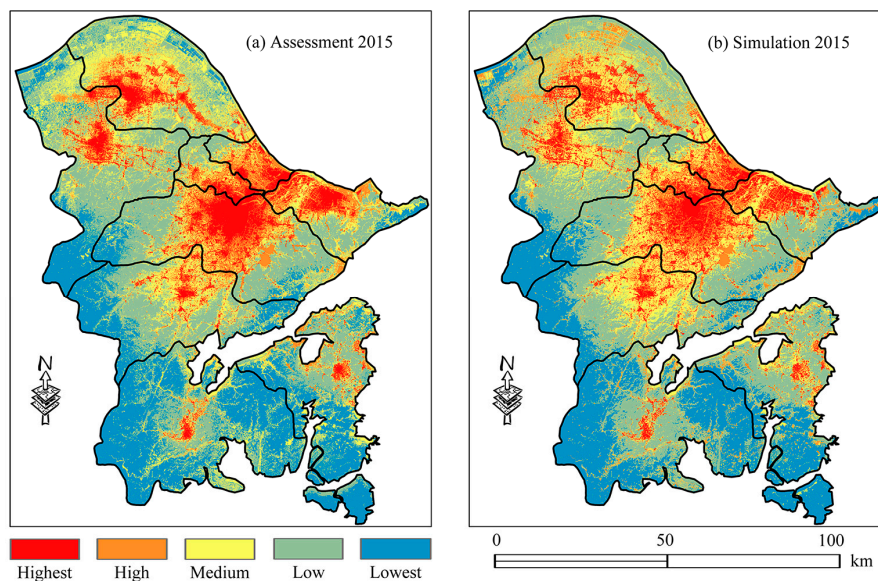


**Figure 7.** Assessment and simulation of 2015 five-level-based RER patterns.

Table 4 shows that overall accuracy is 77.9% and Kappa coefficient is 77.3%, indicating good simulation accuracy of the FLUS model. The producer's and user's accuracies exceed 80% for the "highest," "low" and "lowest" RER levels, and are about 70% for the "high" and "medium" levels. The commission errors are negatively related to the producer's accuracies, while the omission errors are negatively related to the user's accuracies, confirming the effectiveness of the simulation. Overall, the calibrated FLUS model is relatively accurate in simulating the 2015 RER pattern. We therefore applied this model to project the RER scenarios (Figure 8) from 2020 to 2050 at five-year intervals.

**Table 4.** Accuracy and error of future land use simulation (FLUS) simulation of 2015 RER.

ER Level	Overall Accuracy (%)	Kappa Coefficient (%)	Producer's Accuracy (%)	User's Accuracy (%)	Omission Error (%)	Commission Error (%)
Highest			88.9	88.8	11.1	11.2
High			69.4	64.6	30.6	35.4
Medium	77.9	77.3	71.1	71.2	28.9	28.8
Low			81.3	81.3	18.7	18.7
Lowest			85.3	88.3	14.7	11.7

While the overall RER scenario patterns do not show significant changes with time, there is a noticeable trend of increasing RER (Figure 8). The enlarged Beilun area demonstrates the expansion of the "highest" and the "lowest" areas. From 2020 to 2050, there is at least one large patch of "highest" RER in the central area of Ningbo City center, Cixi, Yuyao, Zhenhai and Beilun, whereas the "highest" risk patches in Fenghua, Ninghai and Xiangshan are relatively smaller. The "lowest" RERs occur in southern Yuyao, western Fenghua, and the Ninghai and Xiangshan suburbs.

Our statistics show that the "highest" and "lowest" risk areas will increase, while the other three categories will decrease in the coming 35 years (Table 5). According to our projections, from 2015 to 2050 the "highest" area will increase by 6.8% and the "lowest" area will increase by 9.5%. In contrast, the "high," "medium" and "low" risk categories will decrease in acreage by 4.3%, 4.5%, and 7.6%, respectively. This indicates a possible transformation from the central three risk levels to the most secure (lowest risk) level and the most insecure (highest risk) level over the coming 35 years.

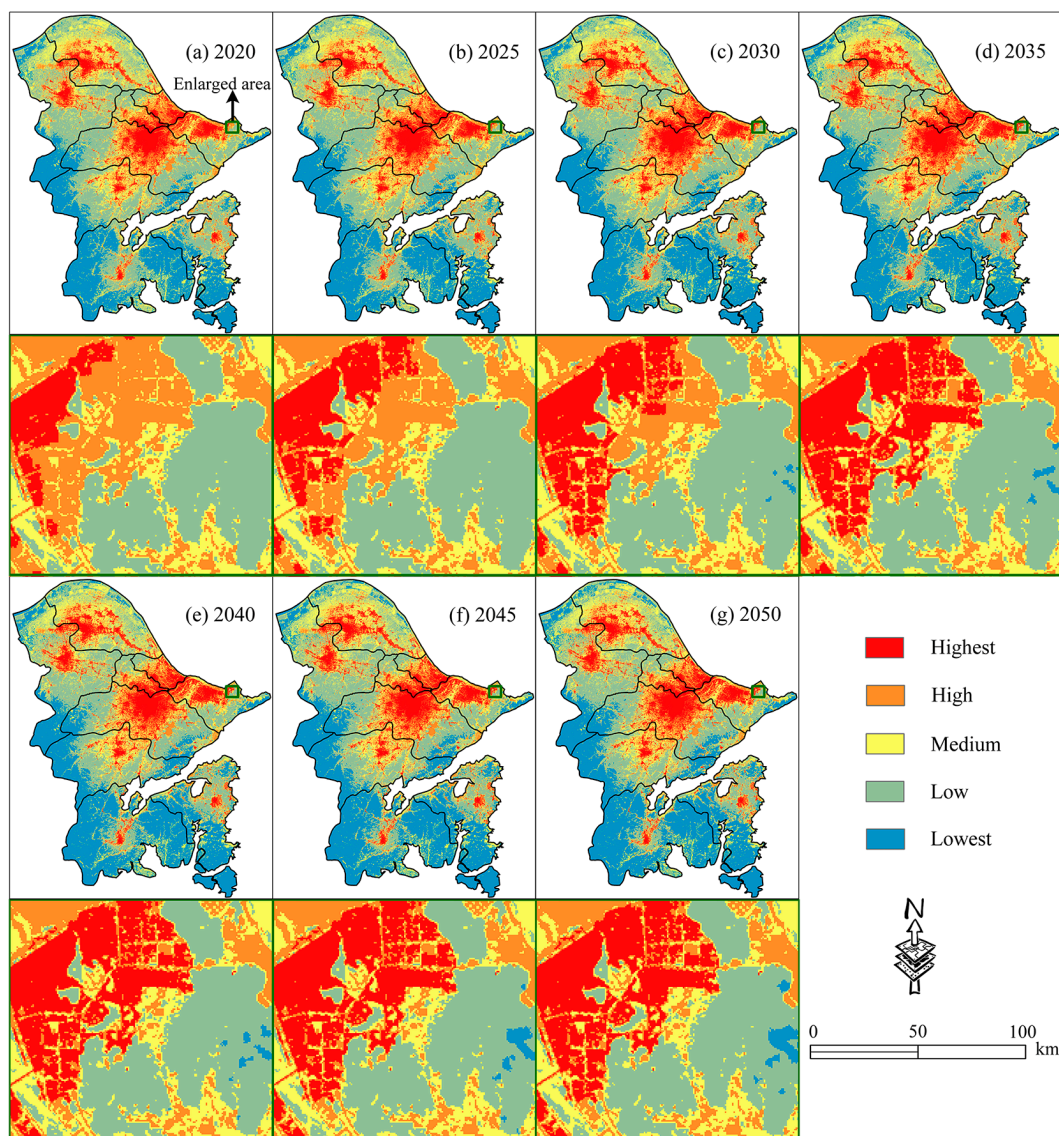


Figure 8. RER future projections at Ningbo from 2020 to 2050.

Table 5. Percentage area for each RER level through time.

Year	Percentage at Each RER Level				
	Highest	High	Medium	Low	Lowest
2015	9.1	10.8	21.6	35.5	23.1
2020	10.0	10.1	21.0	34.4	24.5
2025	11.0	9.5	20.4	33.3	25.8
2030	12.0	8.9	19.7	32.2	27.2
2035	13.0	8.3	19.1	31.0	28.6
2040	13.9	7.7	18.5	30.0	29.9
2045	14.9	7.1	17.8	28.9	31.3
2050	15.9	6.5	17.1	27.9	32.6

### 3.4. Impact of Storm Surge on RER

We used ArcGIS 10.3 to produce the map (Figure 9a) showing the areas affected by the storm surge in the 10 m inundation case, with different color denoting different flooding hours. The map shows that areas closer to the shoreline experience more flooding hours. In a storm surge, most areas of Ningbo are not inundated and are therefore not influenced by the RER. The areas in red are most

affected by the storm surges and are distributed in the low-lying coasts of Yuyao, Cixi, Zhenhai and Beilun, where shoal areas may experience a 20 h inundation.

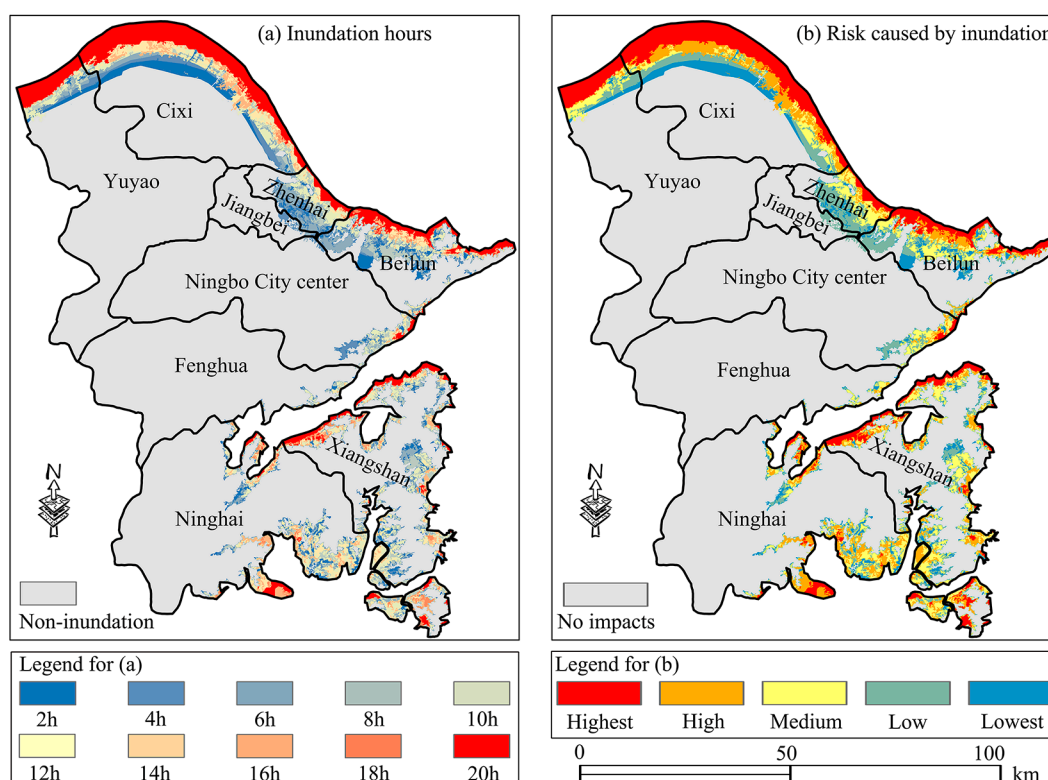


**Figure 9.** Storm-surge-caused RER in the 10 m inundation case: (a) flooding hours; (b) RER related to inundation.

Figure 9a also shows that more than half of Jiangbei and Beilun may endure a 2–10 h inundation, and the coast of Fenghua, Ninghai and Xiangshan will undergo lesser flooding. Table 6 shows the area corresponding to each flooding time and each inundation depth interval. The red areas most likely to be affected by storm surge are about 503 km<sup>2</sup>. In the case of a 10 m inundation, the total area affected by the storm surges reaches about 2104 km<sup>2</sup>, covering 21% of the study area, and the areas under the inundation of 8–14 h are all greater than 200 km<sup>2</sup>.

**Table 6.** Flooding hour and area related to each inundation depth interval.

Flooding Hour	Flooding Area (km <sup>2</sup> ) Corresponding to Different Bathymetry									
	1 m	2 m	3 m	4 m	5 m	6 m	7 m	8 m	9 m	10 m
2	503.6	61.2	172.7	218.9	275.3	231.2	217.8	192.1	100.0	132.0
4	0	503.6	61.2	172.7	218.9	275.3	231.2	217.8	192.1	100.0
6	0	0	503.6	61.2	172.7	218.9	275.3	231.2	217.8	192.1
8	0	0	0	503.6	61.2	172.7	218.9	275.3	231.2	217.8
10	0	0	0	0	503.6	61.2	172.7	218.9	275.3	231.2
12	0	0	0	0	0	503.6	61.2	172.7	218.9	275.3
14	0	0	0	0	0	0	503.6	61.2	172.7	218.9
16	0	0	0	0	0	0	0	503.6	61.2	172.7
18	0	0	0	0	0	0	0	0	503.6	61.2
20	0	0	0	0	0	0	0	0	0	503.6
Total	503.6	564.8	737.5	956.4	1231.7	1462.9	1680.7	1872.8	1972.8	2104.8

Using the correlation between inundation and RER, we mapped the RER pattern caused by a maximum inundation of 10 m (Figure 9b) and calculated the acreage of each level (Table 7). This

confirms the expectation that the region closest to the coastline has a higher RER, displaying a pattern similar to the inundation map. There is an apparent decrease in the RER from the coast to inland areas, indicating a decaying influence of storm surges. The “highest” RER areas (Figure 9b in red) are distributed along the coasts of Yuyao, Cixi and Beilun in the north, but also partially along the coasts of Ninghai and Xiangshan in the south. The area with the “highest” RER accounts for about 6% of the study area (Figure 9b). Inundation-caused RER spreads across about 58% in Zhenhai, with the “medium” to “lowest” levels; whereas RER spreads across about 42% area in Xiangshan, but only 17% in Ninghai.

**Table 7.** RER levels and their area considering the influence of storm surges.

No Impact (km <sup>2</sup> )	Affected Area (km <sup>2</sup> )					Total Area (km <sup>2</sup> )
	Highest	High	Medium	Low	Lowest	
7064.8	564.8	391.6	506.5	409.8	231.9	9169.4

We overlaid the 10 m inundation-caused RER map on the FLUS-projected RER map for each year from 2020 to 2050, producing the overall RER patterns in Figure 10 that consider the combined influence of human activities, land development, SLR, and storm surges. Visual inspection shows no significant differences in RER over time. RER is the highest in the low-lying areas along the coastline in the north and northeast, as well as in the Ningbo City center and district centers. In contrast, there are relatively low RER in Fenghua, Xiangshan and Ninghai. The enlarged area in the Beilun District reveals more detail of the expansion of the “highest” RER. The summary statistics presented in Table 8 confirm this expansion. For example, the “highest” risk areas expand by about 2% from 2020 to 2045 and then remain at 17.7% in the last five years, while the “high” risk areas are reduced by 2% from 2020 to 2040 then remain at 11% from 2040 to 2050. The “medium” RER will stay at ~21% of the study area, while “low” RER areas will decrease by 5%, and the “lowest” RER areas will increase by ~5%. These suggest that human activities, land development, SLR and storm surges will substantially increase the RER at Ningbo.

**Table 8.** Percentage area at each RER level considering the influence of storm surge.

Year	Percentage (%)				
	Highest	High	Medium	Low	Lowest
2020	15.6	13.0	20.9	29.7	20.8
2025	16.1	12.4	21.0	28.9	21.6
2030	16.7	11.9	20.9	28.1	22.4
2035	17.4	11.3	20.8	27.2	23.3
2040	17.6	11.0	20.8	26.4	24.2
2045	17.7	11.0	20.8	25.5	25.0
2050	17.7	11.0	20.7	24.7	25.9

Significant differences exist between the RER scenarios before and after considering the effect of storm surge. As compared with the before-inundation RER (see Table 5), after-inundation RER in the coast of Yuyao, Cixi, Zhenhai and Beilun increases from “lowest” to “highest” level (Table 8). In each year, the after-inundation areas with the “highest” and “high” risks increase by about 4% and 3.4% respectively, and the after-inundation areas with the “lowest” and “low” risks are reduced by about 4% and 5.2% respectively, as compared with the before-inundation RER. This indicates the strong influence of storm surges leading to increased RER, particularly in the low-lying northern coast.

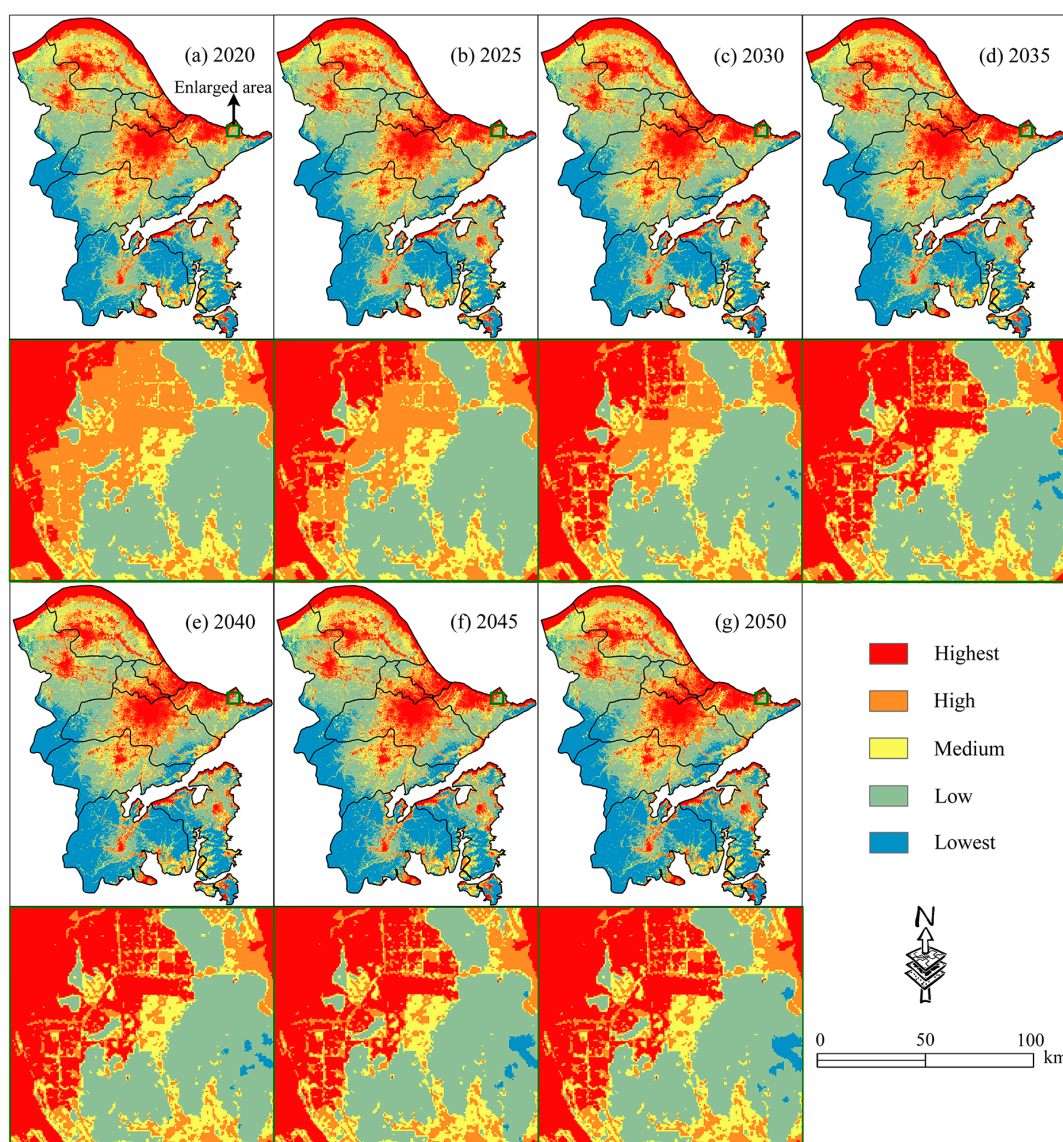


**Figure 10.** Future RER scenarios at Ningbo from 2020 to 2050 that include the influence of 10 m storm-surge inundation.

## 4. Discussion

### 4.1. Our Contribution towards RER Assessment

Spatially explicit assessment and projection of RER are challenging because RER is affected by many factors such as human impacts and global change. We developed a PCA-based approach to evaluate coastal RER patterns considering spatial factors and applied a bottom-up FLUS model to predict future RER scenarios. The historical evaluation (1975–2015) and the future scenario projection (2015–2050) have proved the effectiveness of both the proposed PCA assessment method and the FLUS prediction model.

Compared to earlier publications on RER, our study is featured by the fine-scale assessment and objective parameterization, as well as long-term projection using a CA model considering the influences of SLR and storm surges. The PCA method provided an objective assessment without knowing RER levels prior to modeling, and avoided subjective evaluation that may be caused by AHP and EEM [17,21]. In addition, our 30 m × 30 m grid-based assessment provides more spatial details of the RER as compared with those conducted under larger grids and the administrative

boundaries [21,57]. This may be attributed to the inclusion of the same spatial scale factors such as the land coverage indices and the distance to administrative centers.

Future scenario projection is a crucial issue in RER research. We applied FLUS to project future scenarios based on the classified RER pattern and its driving factors. FLUS is effective in simulating land-use and urban growth [35,37], and our study shows that it can be useful in modeling other spatial phenomena such as RER change. It should be noted that, however, the calibration of the CA-based FLUS model may affect RER simulation and projection. The influencing factors of calibration include the FLUS controlling parameterization, the sampling method, the number of samples, and the neighborhood configuration. While it is unclear how much the calibration may influence the 2015 simulation and future projection, there is a relatively high agreement between the 2015 simulation and assessment. The model shows lower accuracies (~70%) for the “high” and “medium” levels but higher accuracies (>85%) for the “highest” and “lowest” levels. This suggests FLUS may more accurately identify areas with the highest RER, and correctly simulate most of the “lowest” risk areas that should not be included in other categories with higher risks. The calibrated FLUS model is therefore useful in projecting future RER scenarios, and can accurately identify the “highest” RER areas for disaster prevention and the “lowest” RER areas for environmental protection. The future “highest” RER areas also represent an early warning of environmental status change.

#### *4.2. Major Findings and Additional Explanations*

Our results demonstrate that RER at Ningbo has increased substantially over the past 40 years, and will continue to increase slowly in the next 35 years. Ningbo City center and associated district centers experience high RER while the suburbs have relatively lower RER (Figure 4). The historical 40-year RER changes can be attributed to human impacts that are intensified by population growth, rapid urbanization, extensive industrialization, and pollutant emissions [46,58]. RER assessment and ecological security evaluation share similarities, as both measure environmental conditions from a spatial perspective. Our results confirmed early studies that indicated deterioration in the ecosystem and natural environmental conditions at Ningbo [21]. The relatively high RER in Ningbo City center and district centers is mainly caused by human activities and rapid urbanization, accompanied by land surface alteration [40,59]. However, not all the areas studied have experienced increasing RER during the past 40 years. For example, the RER declined in parts of Jiangbei during 1990–2006 (Figure 6b), ascribed to environmental protection and urban park construction.

In addition to technical issues such as the FLUS calibration, the predicted future RER changes will probably be attributable to the aforementioned human impacts, intensifying natural disasters, and global warming. The before-inundation RER scenarios have more negative consequences in the Ningbo City center and district centers, and the after-inundation RER scenarios will significantly increase at the coast, and the RER will be lower in the suburban areas over time. The change may be caused by suburb-to-downtown population migration [60], urban sprawl, and industrialization that produces serious environmental pressures [46], and global change.

#### *4.3. Limitations and Implications*

Our research focused on RER scenario projection by coupling the impact of sea level rise loosely. We produced future scenarios affected by the decadal-scale inundation, considering the topography, bathymetry, and rising water level. This suggests our assessment of after-inundation scenarios is limited in extreme flood events at a specific time point. The process-based FLUS model is not the same category as those for modeling the impacts of the sea level rise. The former model focuses on modeling land-use change and spatial phenomena in terrestrial environments; in contrast, the latter models (e.g., SLAMM, BTELSS, DIVA, and SimCLIM) centralize the dynamic processes in coastal environments and are sophisticated in addressing the sea level rise. To address the dynamic processes in coastal environments, we instead applied a static GIS approach to spatially visualize the inundation by coupling the impacts of sea level rise. Therefore, future RER assessment work should include more

unrelated risk factors and eco-environmental vulnerability on wider regional scales by considering the evolving topo-bathymetry.

This study identifies specific areas with different levels of potential environmental risks by model assessment and projection, providing valuable information for assessing the past urbanization and the environmental protection policies as well as for developing regulations for the management of urban development and coastal environments. For example, Ningbo authorities and urban planners can modify present regulations to achieve a more environmentally friendly city based on our research results. Landscape configuration [61] should be considered intently in residential development to reduce urban stormwater runoff and urban heat island effects, thus mitigating the environmental risk sources. The risks from sea level rise and storm-induced flooding should be closely considered in urban planning, land development, environmental protection and coastal management, thus reducing potential environmental risks and the loss of life and property.

## 5. Conclusions

We developed a PCA-based method for the spatially-explicit assessment of past RER patterns in coastal areas considering the impacts of spatial factors such as land coverage and spatial proximity, and then calibrated the FLUS model to project future RER scenarios by classifying RER patterns into categorical maps. Our evaluation and projection were at a 30 m resolution that provided appropriate spatial detail for effective environmental management. The PCA-based objective evaluation shows that historic RER at Ningbo has substantially increased over the past 40 years, while the FLUS-based projection shows that the future RER will slowly increase over the next 35 years. Inundation-impacted future scenarios can inform us about high RER areas that will probably be most affected by SLR and storm surges. Our research contributes to an improved understanding of the long-term (past and future) changes in RER patterns at Ningbo.

Our contribution towards RER research is the development of the PCA-based assessment method that features objective parameterization as well as the use of the FLUS model for the spatial prediction of future scenarios. The PCA used here is readily applicable to the assessment of RER elsewhere, and should be useful to evaluate the ecological security status. The current RER pattern could help authorities form environmental restoration measures, while the future scenarios are early warnings of impending changes in environmental status, supporting the development of practical policies and regulations for disaster mitigation and environmental protection.

**Author Contributions:** Conceptualization, Y.F.; methodology, Y.F. and Q.Y.; software, Y.F. and Q.Y.; validation, J.W., S.C., Z.L. and C.G.; formal analysis, Y.F. and Q.Y.; investigation, Q.Y.; resources, J.W., S.C., Z.L. and C.G.; data curation, Y.F. and Q.Y.; writing—original draft preparation, Q.Y.; writing—review and editing, Y.F. and X.T.; visualization, J.W., S.C., Z.L. and C.G.; supervision, Y.F. and X.T.; project administration, Y.F. and X.T.; funding acquisition, Y.F. and X.T.

**Funding:** This research was supported by the National Key R&D Program of China (2018YFB0505400 and 2018YFB0505402), and the National Natural Science Foundation of China (41771414 and 41631178).

**Conflicts of Interest:** The authors declare no conflict of interest.

## References

1. Covello, V.T.; Merkhofer, M.W. *Risk Assessment Methods: Approaches for Assessing Health and Environmental Risks*; Plenum Press: New York, NY, USA, 2013; p. 317.
2. Piers, B.; Piers, B.; Terry, C.; Ian, D.; Ben, W. *At Risk: Natural Hazards, People's Vulnerability and Disasters*; Routledge: Abingdon, UK, 2004.
3. Defries, R.S.; Rudel, T.; Uriarte, M.; Hansen, M. Deforestation driven by urban population growth and agricultural trade in the twenty-first century. *Nat. Geosci.* **2010**, *3*, 178–181. [[CrossRef](#)]
4. Liddle, B. Age-structure, urbanization, and climate change in developed countries: Revisiting stirpat for disaggregated population and consumption-related environmental impacts. *Popul. Environ.* **2010**, *31*, 317–343. [[CrossRef](#)]

5. Huang, Q.; Zheng, X.; Hu, Y. Analysis of land-use emergy indicators based on urban metabolism: A case study for Beijing. *Sustainability* **2015**, *7*, 7473–7491. [[CrossRef](#)]
6. Cecchini, M.; Zamboni, I.; Pontrandolfi, A.; Turco, R.; Colantoni, A.; Mavrakis, A.; Salvati, L. Urban sprawl and the 'olive' landscape: Sustainable land management for 'crisis' cities. *Geojournal* **2018**, *84*, 237–255. [[CrossRef](#)]
7. Harley, C.D.G.; Randall Hughes, A.; Hultgren, K.M.; Miner, B.G.; Sorte, C.J.B.; Thornber, C.S.; Rodriguez, L.F.; Tomanek, L.; Williams, S.L. The impacts of climate change in coastal marine systems. *Ecol. Lett.* **2006**, *9*, 228–241. [[CrossRef](#)] [[PubMed](#)]
8. Nicholls, R.J.; Cazenave, A. Sea level rise and its impact on coastal zones. *Science* **2010**, *328*, 1517–1520. [[CrossRef](#)] [[PubMed](#)]
9. Xu, L.; Liu, G. The study of a method of regional environmental risk assessment. *J. Environ. Manag.* **2009**, *90*, 3290–3296. [[CrossRef](#)]
10. Zhang, C.; Li, Y.; Xiong, S.; Lu, X.; Zhu, X. Regional environmental risk assessment and management guide for rapid urbanization process of a city cluster in China. *Hum. Ecol. Risk Assess. Int. J.* **2015**, *22*, 283–301. [[CrossRef](#)]
11. Meng, X.; Zhang, Y.; Yu, X.; Bai, J.; Chai, Y.; Li, Y. Regional environmental risk assessment for the Nanjing chemical industry park: An analysis based on information-diffusion theory. *Stoch. Environ. Res. Risk Assess.* **2014**, *28*, 2217–2233. [[CrossRef](#)]
12. Gretchen, G. Regional risk zonation of environmental pollution on marine and coastal zone. *J. Mar. Environ. Eng.* **2018**, *10*, 97–107.
13. Wang, B.; Cheng, H. Regional Environmental Risk Assessment and Zoning Based on Matrix Method. In Proceedings of the International Conference on Multimedia Technology, Hangzhou, China, 26–28 July 2011; pp. 1644–1647.
14. Albanese, S.; Vivo, B.D.; Lima, A.; Frattasio, G.; Křibek, B.; Nyambe, I.; Majer, V. Prioritising environmental risk at the regional scale by a gis aided technique: The zambian copperbelt province case study. *J. Geochem. Explor.* **2014**, *144*, 433–442. [[CrossRef](#)]
15. Jiang, S.; Zhai, Y.; Leng, S.; Wang, J.; Teng, Y. A hive model for regional integrated environmental risk assessment: A case study in China. *Hum. Ecol. Risk Assess. Int. J.* **2015**, *22*, 1002–1028. [[CrossRef](#)]
16. Minolfi, G.; Albanese, S.; Lima, A.; Tarvainen, T.; Fortelli, A.; Vivo, B.D. A regional approach to the environmental risk assessment–human health risk assessment case study in the campania region. *J. Geochem. Explor.* **2016**, *184*, 400–416. [[CrossRef](#)]
17. Narimisa, M.R.; Narimisa, M.R. The research of environmental impact assessment for oil refineries in Iran based on AHP and GIS. *J. Hum. Cult. Stud.* **2016**, *1*, 1396–1416.
18. Jozi, S.A.; Shafiee, M.; Moradimajd, N.; Saffarian, S. An integrated shannon's entropy-topsis methodology for environmental risk assessment of helleh protected area in Iran. *Environ. Monit. Assess.* **2012**, *184*, 6913–6922. [[CrossRef](#)] [[PubMed](#)]
19. Sadiq, R.; Husain, T. A fuzzy-based methodology for an aggregative environmental risk assessment: A case study of drilling waste. *Environ. Model. Softw.* **2005**, *20*, 33–46. [[CrossRef](#)]
20. Feng, Y.; Liu, Y.; Liu, Y. Spatially explicit assessment of land ecological security with spatial variables and logistic regression modeling in Shanghai, China. *Stoch. Environ. Res. Risk Assess.* **2017**, *31*, 2235–2249. [[CrossRef](#)]
21. Feng, Y.; Yang, Q.; Tong, X.; Chen, L. Evaluating land ecological security and examining its relationships with driving factors using GIS and generalized additive model. *Sci. Total Environ.* **2018**, *633*, 1469–1479. [[CrossRef](#)]
22. Sampath, D.M.R.; Boski, T.; Loureiro, C.; Sousa, C. Modelling of estuarine response to sea-level rise during the holocene: Application to the Guadiana Estuary–SW Iberia. *Geomorphology* **2015**, *232*, 47–64. [[CrossRef](#)]
23. Webb, A.P.; Kench, P.S. The dynamic response of reef islands to sea-level rise: Evidence from multi-decadal analysis of island change in the central Pacific. *Glob. Planet. Chang.* **2010**, *72*, 234–246. [[CrossRef](#)]
24. Stralberg, D.; Brennan, M.; Callaway, J.C.; Wood, J.K.; Schile, L.M.; Jongsomjit, D.; Kelly, M.; Parker, V.T.; Crooks, S. Evaluating tidal marsh sustainability in the face of sea-level rise: A hybrid modeling approach applied to san francisco bay. *PLoS ONE* **2011**, *6*, e27388. [[CrossRef](#)]
25. McLeod, E.; Poulter, B.; Hinkel, J.; Reyes, E.; Salm, R. Sea-level rise impact models and environmental conservation: A review of models and their applications. *Ocean Coast. Manag.* **2010**, *53*, 507–517. [[CrossRef](#)]

26. Wahl, T.; Jain, S.; Bender, J.; Meyers, S.D.; Luther, M.E. Increasing risk of compound flooding from storm surge and rainfall for major us cities. *Nat. Clim. Chang.* **2015**, *5*, 1093. [CrossRef]
27. Mevik, B.-H.; Wehrens, R.; Liland, K.H. PLS: Partial least squares and principal component regression. Available online: <https://cran.r-project.org/web/packages/pls/index.html> (accessed on 14 March 2019).
28. Akgun, A.; Kincal, C.; Pradhan, B. Application of remote sensing data and gis for landslide risk assessment as an environmental threat to Izmir city (west Turkey). *Environ. Monit. Assess.* **2012**, *184*, 5453–5470. [CrossRef]
29. Aydi, A.; Zairi, M.; Dhia, H.B. Minimization of environmental risk of landfill site using fuzzy logic, analytical hierarchy process, and weighted linear combination methodology in a geographic information system environment. *Environ. Earth Sci.* **2013**, *68*, 1375–1389. [CrossRef]
30. Santini, M.; Caccamo, G.; Laurenti, A.; Noce, S.; Valentini, R. A multi-component gis framework for desertification risk assessment by an integrated index. *Appl. Geogr.* **2010**, *30*, 394–415. [CrossRef]
31. Ali-Akbarpour, M.; Mohammadbeigi, A.; Tabatabaee, S.H.R.; Hatam, G. Spatial analysis of eco-environmental risk factors of cutaneous leishmaniasis in southern Iran. *J. Cutan. Aesthet. Surg.* **2012**, *5*, 30–35.
32. Lahr, J.; Kooistra, L. Environmental risk mapping of pollutants: State of the art and communication aspects. *Sci. Total Environ.* **2010**, *408*, 3899–3907. [CrossRef]
33. Wang, M.; Bai, Y.; Chen, W.; Markert, B.; Peng, C.; Ouyang, Z. A GIS technology based potential eco-risk assessment of metals in urban soils in Beijing, china. *Environ. Pollut.* **2012**, *161*, 235–242. [CrossRef]
34. Feng, Y.; Liu, Y.; Tong, X. Comparison of metaheuristic cellular automata models: A case study of dynamic land use simulation in the Yangtze River delta. *Comput. Environ. Urban Syst.* **2018**, *70*, 138–150. [CrossRef]
35. Liu, X.; Liang, X.; Li, X.; Xu, X.; Ou, J.; Chen, Y.; Li, S.; Wang, S.; Pei, F. A future land use simulation model (FLUS) for simulating multiple land use scenarios by coupling human and natural effects. *Landsc. Urban Plan.* **2017**, *168*, 94–116. [CrossRef]
36. Feng, Y. Modeling dynamic urban land-use change with geographical cellular automata and generalized pattern search-optimized rules. *Int. J. Geogr. Inf. Sci.* **2017**, *31*, 1198–1219.
37. Liang, X.; Liu, X.; Li, X.; Chen, Y.; Tian, H.; Yao, Y. Delineating multi-scenario urban growth boundaries with a ca-based flus model and morphological method. *Landsc. Urban Plan.* **2018**, *177*, 47–63. [CrossRef]
38. Wu, Y.; Chen, Y.; Deng, X.; Hui, E.C.M. Development of characteristic towns in china. *Habitat Int.* **2018**, *77*, 21–31. [CrossRef]
39. Ningbo Municipal Statistics Bureau. *Ningbo Statistical Yearbook in 2015*; Ningbo Municipal Statistics Bureau: Ningbo, China, 2016.
40. Liu, R.; Borthwick, A.G. Measurement and assessment of carrying capacity of the environment in Ningbo, China. *J. Environ. Manag.* **2011**, *92*, 2047–2053. [CrossRef]
41. Wang, D.; Luo, Z.; Zhang, X.; Lin, L.; Du, M.; Laing, G.D.; Yan, C. Occurrence, distribution and risk assessment of estrogenic compounds for three source water types in Ningbo city, China. *Environ. Earth Sci.* **2015**, *74*, 5961–5969. [CrossRef]
42. Feng, Y.; Yang, Q.; Hong, Z.; Cui, L. Modelling coastal land use change by incorporating spatial autocorrelation into cellular automata models. *Geocarto Int.* **2016**, *33*, 470–488. [CrossRef]
43. Zheng, Q.; Yang, X.; Wang, K.; Huang, L.; Shahtahmassebi, A.R.; Gan, M.; Weston, M.V. Delimiting urban growth boundary through combining land suitability evaluation and cellular automata. *Sustainability* **2017**, *9*, 2213. [CrossRef]
44. Wang, H.; Long, H.; Li, X.; Yu, F. Evaluation of changes in ecological security in china's qinghai lake basin from 2000 to 2013 and the relationship to land use and climate change. *Environ. Earth Sci.* **2013**, *72*, 341–354. [CrossRef]
45. Liu, X.; Li, X.; Chen, Y.; Tan, Z.; Li, S.; Ai, B. A new landscape index for quantifying urban expansion using multi-temporal remotely sensed data. *Landsc. Ecol.* **2010**, *25*, 671–682. [CrossRef]
46. Liu, Y.; Feng, Y. Simulating the impact of economic and environmental strategies on future urban growth scenarios in Ningbo, China. *Sustainability* **2016**, *8*, 1045. [CrossRef]
47. Zheng, R.; Liu, Y.; Dong, Y.; Zhu, G. Appraisal of land resources security in guangzhou based on major function regionalization. *Acta Geogr. Sin.* **2009**, *6*, 654–664.
48. Hopping, K.A.; Yeh, E.T.; Harris, R.B. Linking people, pixels, and pastures: A multi-method, interdisciplinary investigation of how rangeland management affects vegetation on the Tibetan plateau. *Appl. Geogr.* **2018**, *94*, 147–162. [CrossRef]

49. Zheng, Y.; Ren, C.; Xu, Y.; Wang, R.; Ho, J.; Lau, K.; Ng, E. GIS-based mapping of local climate zone in the high-density city of Hong Kong. *Urban Clim.* **2017**, *24*, 419–448. [[CrossRef](#)]
50. Wellmann, T.; Haase, D.; Knapp, S.; Salbach, C.; Selsam, P.; Lausch, A. Urban land use intensity assessment: The potential of spatio-temporal spectral traits with remote sensing. *Ecol. Indic.* **2018**, *85*, 190–203. [[CrossRef](#)]
51. Wenskovitch, J.; Crandell, I.; Ramakrishnan, N.; House, L.; Leman, S.; North, C. Towards a systematic combination of dimension reduction and clustering in visual analytics. *IEEE Trans. Vis. Comput. Graph.* **2018**, *24*, 131–141. [[CrossRef](#)]
52. Sui, L.; Zheng, J.; Yu, J.; Wang, X. Comprehensive evaluation on shale fracability using principal component analysis. *Electron. J. Geotech. Eng.* **2015**, *20*, 5965–5976.
53. Halmy, M.W.A.; Gessler, P.E.; Hicke, J.A.; Salem, B.B. Land use/land cover change detection and prediction in the north-western coastal desert of Egypt using markov-ca. *Appl. Geogr.* **2015**, *63*, 101–112. [[CrossRef](#)]
54. State Ocean Administration of China. The Bulletin of Sea Level in China in 2011. Available online: [http://www.soa.gov.cn/zwgk/hygb/zghpmgb/201211/t20121105\\_5568.html](http://www.soa.gov.cn/zwgk/hygb/zghpmgb/201211/t20121105_5568.html) (accessed on 5 May 2018).
55. Shi, Y. Trends of natural disasters in china under global warming. *J. Nat. Disaster* **1996**, *5*, 102–116.
56. Ravela, S.; Neumann, J.E.; Verly, C.; Ludwig, L.C.; Emanuel, K.A. Risks of coastal storm surge and the effect of sea level rise in the red river delta, Vietnam. *Sustainability* **2015**, *7*, 6553–6572.
57. Yu, G.; Zhang, S.; Yu, Q.; Fan, Y.; Zeng, Q.; Wu, L.; Zhou, R.R.; Nan, N.; Zhao, P. Assessing ecological security at the watershed scale based on RS/GIS: A case study from the Hanjiang River basin. *Stoch. Environ. Res. Risk Assess.* **2014**, *28*, 307–318. [[CrossRef](#)]
58. He, T.; Yang, Z.; Tao, L.; Shen, Y.; Fu, X.; Qian, X.; Zhang, Y.; Yong, W.; Xu, Z.; Zhu, S. Ambient air pollution and years of life lost in Ningbo, China. *Sci. Rep.* **2016**, *6*, 22485. [[CrossRef](#)]
59. Liu, Y.L.; Feng, Y.H.; Zhe, Z.; Zhang, Q.W.; Su, S.L. Socioeconomic drivers of forest loss and fragmentation: A comparison between different land use planning schemes and policy implications. *Land Use Policy* **2016**, *54*, 58–68. [[CrossRef](#)]
60. McKinsey Global Institute. Preparing for China’s Urban Billions. Available online: <https://www.Mckinsey.Com/mgi/overview> (accessed on 5 May 2018).
61. Feng, Y.; Liu, Y.; Tong, X. Spatiotemporal variation of landscape patterns and their spatial determinants in shanghai, china. *Ecol. Indic.* **2018**, *87*, 22–32. [[CrossRef](#)]



© 2019 by the authors. Licensee MDPI, Basel, Switzerland. This article is an open access article distributed under the terms and conditions of the Creative Commons Attribution (CC BY) license (<http://creativecommons.org/licenses/by/4.0/>).